Ab initio typical medium theory of substitutional disorder

A. Östlin,[1] Y. Zhang,[2,3] H. Terletska,[4] F. Beiuşeanu,[5] V. Popescu,[6] K. Byczuk,[7] L. Vitos,[8,9,10] M. Jarrell,[2,*] D. Vollhardt,[1] and L. Chioncel[1,11]

[1]*Theoretical Physics III, Center for Electronic Correlations and Magnetism, Institute of Physics, University of Augsburg, D-86135 Augsburg, Germany*

[2]*Department of Physics & Astronomy and Center for Computation & Technology, Louisiana State University, Baton Rouge, Louisiana 70803, USA*

[3]*Kavli Institute for Theoretical Sciences, Beijing 100190, China*

[4]*Department of Physics and Astronomy, Middle Tennessee State University, Murfreesboro, Tennessee 37132, USA*

[5]*Faculty of Science, University of Oradea, RO-410087 Oradea, Romania*

[6]*Sophie-Scholl-Gymnasium Oberhausen, 46145 Oberhausen, Germany*

[7]*Institute of Theoretical Physics, Faculty of Physics, University of Warsaw, ul. Pasteura 5, PL-02-093 Warszawa, Poland*

[8]*Department of Materials Science and Engineering, Applied Materials Physics, KTH Royal Institute of Technology, SE-10044 Stockholm, Sweden*

[9]*Department of Physics and Materials Science, Division for Materials Theory, Uppsala University, SE-75121 Uppsala, Sweden*

[10]*Research Institute for Solid State Physics and Optics, Hungarian Academy of Sciences, P.O. Box 49, H-1525 Budapest, Hungary*

[11]*Augsburg Center for Innovative Technologies, University of Augsburg, D-86135 Augsburg, Germany*

(Received 5 November 2019; published 29 January 2020)

By merging single-site typical medium theory with density-functional theory, we introduce a self-consistent framework for electronic-structure calculations of materials with substitutional disorder which takes into account Anderson localization. The scheme and details of the implementation are presented and applied to the hypothetical alloy Li_cBe_{1-c}, and the results are compared with those obtained with the coherent potential approximation. Furthermore, we demonstrate that Anderson localization suppresses ferromagnetic order for a very low concentration of (i) carbon impurities substituting oxygen in $MgO_{1-c}C_c$ and (ii) manganese impurities substituting magnesium in $Mg_{1-c}Mn_cO$ for the low-spin magnetic configuration.

DOI: 10.1103/PhysRevB.101.014210

I. INTRODUCTION

The unusual electronic properties of disordered metals and alloys [1–3] result from the absence of translational invariance in such systems. To calculate the physical properties of disordered solids and, in particular, to determine their electronic structure is still a challenging problem which involves the sampling of random configurations followed by a quantum-mechanical computation for each disorder configuration. Disordered systems are usually modeled numerically by large supercells in real space, where the results must then be averaged over different realizations of the disorder. This increases the cost of electronic-structure calculations of disordered systems considerably.

In this paper, we introduce a computational approach which merges effective-medium approximations with the density-functional theory [4–8] (DFT) to investigate structurally disordered solids. The effective medium is calculated by means of a statistical approach, which takes into account the strength of the disordered alloy potential. The latter can be decomposed into a sum of contributions from the individual atomic scatterers, such that the electron propagation can be viewed as a succession of scatterings from these atomic potentials. The essence of the effective–medium theory is the self-consistent treatment of the multiple-scattering events: The scatterers are viewed as embedded in an effective medium whose properties still have to be determined. If the average scattering from a single impurity in the presence of the effective medium is set to zero, one obtains the well-known coherent potential approximation (CPA) [1,9]. The CPA was introduced by Soven [10] and Taylor [11] to study electronic and vibrational properties of random alloys, respectively. It was then further developed and extensively applied to disordered solids [1–3,9,12]. To investigate the electronic structure of realistic materials Győrffy [13] formulated the CPA in the framework of multiple scattering theory by using the Green's function technique.

Even today the CPA is one of the most widely employed methods to calculate the electronic structure of random alloys. Numerous applications [14–23] have shown that within this approximation one can calculate lattice parameter, bulk modulus, mixing enthalpy, etc., with an accuracy similar to that obtained for ordered solids. At the same time the applicability of the CPA is limited since it is a single-site approximation. For example, CPA neither takes into account disorder–induced short-range correlations, nor the effects of Anderson localization [2]. Furthermore, systems with a large size mismatch between the alloy components are difficult to treat within CPA because of the local lattice relaxations. The search for

[*]Deceased.

a generalization of the CPA has proven to be difficult. There have been numerous attempts to overcome the main shortcomings of the CPA by incorporating the missing nonlocal physics, e.g., by employing the molecular CPA [24,25] and the dynamical cluster approximation (DCA) [26] in model Hamiltonian calculations, and the KKR-nonlocal coherent potential approximation (KKR-NLCPA) [27–30], where the DCA coarse graining approach is applied.

The purpose of the present paper is to introduce an alternative choice of the effective medium, which is able to take into account the effects of Anderson localization even in a real disordered material, by formulating it within the framework of DFT. As pointed out by Anderson [31], the key quantity to study in a disordered system is the amplitude of the electronic wave functions. At the localization transition the Hamiltonian spectrum in the vicinity of a given energy changes from continuous to discrete (dense-pointlike) in the thermodynamic limit and the *typical*, i.e., the most probable value of the local density of states (LDOS) at this energy, vanishes. The typical value of the LDOS is well represented by the geometric average [32] $\rho_{\rm typ}(E) = \exp[\langle \ln \ \rho_i(E)\rangle]$, where $\langle ...\rangle$ represents the arithmetic average over disorder and $\rho_i(E)$ is the LDOS at site i for the energy E [33]. This technique was successfully applied to model Hamiltonians and is referred to as typical medium theory (TMT) [34–40]. The TMT can describe signatures of Anderson localization in the spectral function, i.e., on the one-particle level, but does not capture short-range order effects.

Recently, the typical medium dynamical cluster approximation (TMDCA) [41,42] was introduced, which extends the single-site TMT to a finite cluster and allows for a systematic inclusion of the nonlocal multisite correlations. It was shown that the TMDCA overcomes many shortcomings of the TMT since it allows one to identify effects of Anderson localization in higher-order correlation functions, e.g., the conductivity. This method has also been extended to models with off-diagonal disorder [43], multiband systems [44], and interactions [45]. To go beyond model studies and also ultimately investigate real materials, the TMDCA was subsequently formulated within the framework of multiple scattering theory [46]. However, so far this framework was only applied to model Hamiltonians [41,42,44]. While some of these models were extracted from first-principles calculations [44,47,48], no self-consistent feedback between the models and the typical medium analysis was considered.

The aim of our paper is to extend this methodology from models to realistic three-dimensional muffin-tin systems by merging the single-site TMT with DFT.

The paper is organized as follows. In Sec. II, we introduce two effective medium theories which have been formulated to compute electronic structures using Green's functions. In Sec. III, we review the theory using the exact muffin-tin orbitals (EMTO) basis set and present the form of the Green's function and path operators. The CPA- and TMT-Green's function condition for the self-consistency of the effective medium are discussed in Sec. III B. The method is then applied to compute the electronic properties of the hypothetical Li_cBe_{1-c} alloy and the dilute $MgO_{1-c}C_c$ and $Mg_{1-c}Mn_cO$ alloys. The Li-Be system is used as an illustrative example to compare CPA vs TMT calculations, and to discuss signatures of the precursor of the Anderson localization transition. In the dilute $MgO_{1-c}C_c$ and $Mg_{1-c}Mn_cO$ alloys, we investigate how magnetism is influenced by weak disorder (within CPA) and strong disorder (within TMT), respectively.

II. SINGLE-SITE EFFECTIVE-MEDIUM THEORIES

We begin with a general description of the effective-medium theory of realistic multiatom alloys. To this end, we consider a substitutional alloy $A_aB_bC_c...$, where the atoms A, B, C,... are randomly distributed on the underlying crystal structure. Here a, b, c, ... stand for the atomic fractions (concentrations) of the A, B, C,... atoms, respectively. In the alloy, it is assumed that the potential of the atoms at any lattice site is completely random and can be described by a probability distribution function (PDF) $P(\epsilon_1, ...\epsilon_N)$ for local energy levels ϵ_i, where N is the total number of atoms in the sample. This allows us to determine the expectation value of an observable $\mathcal{A}(\epsilon_1, ..., \epsilon_N)$ as the arithmetic average over different disorder realizations with this PDF, i.e., $\tilde{\mathcal{A}} = \langle \mathcal{A} \rangle_{\rm arith} = \int_{-\infty}^{\infty} \prod_{i=1}^{N} d\epsilon_i \mathcal{A}(\epsilon_1, ..., \epsilon_N) P(\epsilon_1, ..., \epsilon_N)$.

There are two major approximations in the single-site effective medium construction: (i) the local potentials around one type of atoms forming the alloy are assumed to be the same, i.e., the effect of the local environment is neglected. Therefore, the PDF is uncorrelated and has a product form, where the PDF for each type of atom is given by $P_{\rm A}, P_{\rm B}, P_{\rm C}, ...$, respectively [49], and (ii) the system is replaced by a monoatomic effective crystal described by the site-independent "effective medium potential" $\tilde{D}$. One therefore approximates the Green's function g of a real system by an "effective medium Green's function" $\tilde{g}$, and for each alloy component $j = $ A, B, C,... a single-site Green's function g_j is determined. The construction of such a single-site effective medium involves the following steps:

(1) The effective Green's function is calculated from the effective potential using an electronic structure method. For example, within the Korringa-Kohn-Rostoker (KKR) [25,50–54] or linear muffin-tin orbital (LMTO) [55,56] methods, one has

$$\tilde{g} = [S - \tilde{D}]^{-1}, \tag{1}$$

where S denotes the KKR or LMTO structure constant matrix corresponding to the underlying lattice.

(2) Next, the Green's functions g_j of the alloy components are determined by substituting the real atomic potentials D_j by their value computed with respect to the effective medium potential $\tilde{D}$. Mathematically, this condition is expressed by the real-space Dyson equation

$$g_j = \tilde{g} + \tilde{g}(D_j - \tilde{D})g_j, \quad j = \text{A, B, C....} \tag{2}$$

(3) Finally, the average of the individual Green's functions should reproduce the single-site part of the effective medium Green's function, i.e.,

$$\tilde{g} = \tilde{g}[g_{\rm A}, g_{\rm B}, g_{\rm C}, ...]. \tag{3}$$

This functional relation needs to be specified for each type of effective medium theory.

Equations (1)–(3) are solved iteratively, and the output functions $\tilde{g}$ and g_j are used to determine the electronic structure, charge density, and the total energy of the random alloy.

If $\tilde{g}$ is determined by the arithmetic average the results are equivalent to the CPA and are insensitive to Anderson localization. By contrast, the geometric average leads to the TMT, which is capable of describing disorder-driven Anderson localization effects. In the next section, we will present this construction for the TMT explicitly.

III. EFFECTIVE MEDIUM THEORY USING EXACT MUFFIN-TIN ORBITALS

The EMTO theory [57,58] formulates an efficient and at the same time accurate muffin-tin method for solving the Kohn-Sham equations [4,5] of the DFT [4–8]. By using large overlapping potential spheres, the EMTO approach describes the exact crystal potential more accurately than any other conventional muffin-tin method. In the EMTO approach, while keeping the simplicity and efficiency of the muffin-tin formalism, the one-electron states are determined exactly for the model potential.

A. Effective medium potential

Within the overlapping muffin-tin approximation, the Kohn-Sham effective potential $v(\mathbf{r})$ for a real alloy is approximated by spherical potential wells $v_R^j(r_R)$ centered on atomic sites $\mathbf{R}$, where the subscript j denotes the alloy component at site $\mathbf{R}$, supplemented by a constant interstitial potential v_0, i.e.,

$$v(\mathbf{r}) \approx v_{\rm mt}(r) \equiv v_0 + \sum_R \left[v_R^j(r_R) - v_0\right]. \tag{4}$$

Here we introduced the notation $\mathbf{r}_R \equiv \mathbf{r} - \mathbf{R} \equiv r_R \hat{r}_R$, where $\hat{r}_R = \mathbf{r}_R/|\mathbf{r}_R|$, and $r_R = |\mathbf{r}_R|$. In the following, we will omit the explicit vector notation for simplicity.

Next we consider a substitutional alloy with a fixed underlying lattice. We denote the positions of the atoms of the underlying lattice by R, R', etc. in a given unit cell. Within the unit cell we can have one of the atoms from the N_R components forming an alloy, e.g., for a binary-alloy $N_R = 2$. The atomic fractions of the components determine the concentrations c_R^j ($j = 1, 2, ..., N_R$). The individual spherical potentials in Eq. (4), denoted by $v_R^j(r_R)$, are defined within the potential spheres of radii s_R^j. We note that these potentials are not exactly the same as the spherical potentials present in a real alloy because of different local environments. Within effective medium theories, we assume that all potential-dependent functions, such as the partial waves, logarithmic derivatives, normalization functions, etc., belonging to the same kind of atom within a given unit cell, are the same.

The effective medium is described by a site-dependent effective potential (subscript R), which possesses the symmetry of the underlying crystal lattice.

B. Effective medium Green's function

In the EMTO formalism, the effective potential is introduced via the logarithmic derivative $\tilde{D}_{RL'RL}(z)$ of the effective scatterers. Therefore, the coherent Green's function or the path operator Eq. (1) is given by [58]

$$\sum_{R''L''} a_{R'}[S_{R'L'R''L''}(\kappa^2, \mathbf{k}) - \delta_{R'R''}\tilde{D}_{R'L'R'L''}(z)] \times \tilde{g}_{R''L''RL}(z, \mathbf{k}) = \delta_{R'R}\delta_{L'L}, \tag{5}$$

where $l, l', l'' \leqslant l_{\max}$, and $S_{R'L'R''L''}(\kappa^2, \mathbf{k})$ are the elements of the EMTO slope matrix for complex energy $\kappa^2 = z - v_0$ and Bloch vector $\mathbf{k}$ from the Brillouin zone (BZ). The logarithmic derivative of the effective scatterers is site-diagonal with nonzero $L' \neq L$ off-diagonal elements.

The local part of the Green's function of the alloy component $g^j_{RL,RL'}$ is calculated as an impurity Green's function embedded in the effective medium. In the single-site approximation, this is obtained from the real-space Dyson equation [Eq. (2)] as a single-site perturbation on the coherent potential as

$$g^j_{RLRL'}(z) = \tilde{g}_{RLRL'}(z) + \sum_{L''L'''} \tilde{g}_{RLRL''}(z) \times \left[D^j_{Rl''}(z)\delta_{L''L'''} - \tilde{D}_{RL''RL'''}(z)\right] g^j_{RL'''RL'}(z). \tag{6}$$

Here $D^j_{Rl}(z)$ is the logarithmic derivative function for the jth alloy component and $\tilde{g}_{RLRL'}(z) = \int_{\rm BZ} \tilde{g}_{RL,RL'}(z, \mathbf{k}) d\mathbf{k}$ is the site-diagonal part of the $\mathbf{k}$-integrated effective medium Green's function. The condition of zero average scattering leads to a functional relation between $\tilde{g}_{RLRL'}(z)$ and the Green's functions of alloy components, namely,

$$\tilde{g}_{RLRL'}(z) = \tilde{g}\left[g^j_{RLRL'}(z)\right], \tag{7}$$

which still needs to be specified for different types of effective medium theories (see below). Equations (5), (6), and (7) are solved self-consistently for $\tilde{D}(z)$, $\tilde{g}(z, \mathbf{k})$, and $g^j(z)$. Note that the Green's functions for the alloy component and effective medium denoted as g^j and $\tilde{g}$, respectively, carry the information about the poles. Using the partial waves, the Green's functions are properly normalized.

As discussed earlier, there are two possibilities for determining properties of the effective medium:

(i) *The coherent potential condition* provides an expression for the coherent path operator $\tilde{g}$ as the algebraic average of the alloy-component path operators g^j for an arbitrary complex argument z, i.e.,

$$\tilde{g}_{RLRL'}(z) := g^{\rm CPA}_{RL,RL'}(z) = \sum_j c_R^j \, g^j_{RL,RL'}(z). \tag{8}$$

Obviously, the same algebraic condition is simultaneously fulfilled by the real and imaginary parts of this coherent path operator.

(ii) By contrast, the *typical medium condition* is formulated along the real energy axis, i.e., the geometrical average is given by

$$\rho^{\rm TMT}_{RL}(E) := \prod_j \left[\rho^j_{RL}(E)\right]^{c_R^j}. \tag{9}$$

Since the LDOS is defined only for real energies E, it has to be computed at each iteration of the typical medium self-consistency loop. This makes it necessary to perform analytic

continuations between the complex-plane point z and the real-axis point E. To avoid the repetitive and CPU time consuming analytic continuation, we perform the geometric averaging in the current implementation in the complex-plane and define the path operator as

$$g^{\rm TMT}_{RL,RL}(z) := \prod_j \left[g^j_{RL,RL}(z)\right]^{c^j_R}. \tag{10}$$

Along the real axis Eq. (10) multiplied with the normalization of the partial waves (which is real on the real axis) provides the LDOS $\rho^j_{RL}(E)$. We note that in general the condition expressed by Eq. (10) is an approximation to the TMT condition Eq. (9).

With this prescription of how to determine the effective medium in terms of the path operator, the expression for the LDOS for a specific impurity j at site R is determined from

$$\rho^j_{RL}(z) \equiv -\frac{1}{\pi}\Im\left\{\int_{\rm BZ}\sum_{R'L'}\tilde{g}_{RLR'L'}(z,\mathbf{k})\, a_{R'}\dot{S}_{R'L'RL}(\kappa^2,\mathbf{k})d\mathbf{k} - g^j_{RLRL}(z)\dot{D}^j_{Rl}(z) - \mathcal{G}^{j,p}_{Rl}(z)\right\}, \tag{11}$$

where the overdot denotes the energy derivative. The off-diagonal ($R \neq R'$) elements of the coherent Green's function $\tilde{g}_{R'L'RL}(z,\mathbf{k})$ are calculated from Eq. (5) with the self-consistently determined logarithmic derivative $\tilde{D}_{RL'RL}(z)$ of the effective scatterers. The first and second terms on the right-hand side of Eq. (11) assure the proper normalization of the one-electron states for the optimized overlapping potential. The third term in Eq. (11) removes the unphysical pole of the logarithmic derivative. This is a specific step in the EMTO implementation [58]. Altogether, the three terms provide the EMTO Green's function of the effective medium. The search for the Fermi level is similar to the standard CPA procedure as implemented in the EMTO [58].

IV. APPLICATIONS

We now apply the CPA-EMTO and TMT-EMTO theories to the hypothetical alloy Li_cBe_{1-c} as well as to $MgO_{1-c}C_c$ and $Mg_{1-c}Mn_cO$ in the dilute limit (low concentrations c) and compare the results. The motivation to study the LiBe system comes from the fact that it represents a simple cubic system with one atom per unit cell, for which the different effective-medium averaging procedures can be tested readily. At the same time, it also allows one to identify features of the LDOS which can be traced back to effects of Anderson localization. Our choice of MgO is motivated by the relatively large insulating gap. Spin-polarized in-gap states are formed upon carbon and manganese substitutions in MgO, an effect that is sometimes linked to the so-called d^0 magnetism [59,60]. We will show that such an effect can be reproduced within the CPA. However, self-consistent TMT calculations provide a different picture, namely, that fluctuations in the number of particles influence the magnetic stability. In addition to localization, the spin polarization is significantly reduced.

A. Li_cBe_{1-c} alloys: An illustrative example

In pure Li and Be, the atomic s orbitals form a single band. In Be, by partial substitution with Li, the local energies become statistically independent (random) variables with a distribution function

$$P(\epsilon_i) = c_{\rm Li}\delta(\epsilon_i - \epsilon_{\rm Li}) + c_{\rm Be}\delta(\epsilon_i - \epsilon_{\rm Be}),$$

where $c_{\rm Li}$ and $c_{\rm Be}$ are the concentration of Li and Be in the alloy, respectively. The bandwidth is determined by the magnitude of the intersite hopping and the coordination number. Anderson [31] discovered that when the width Γ of the distribution $P(\epsilon_i)$ is smaller than a critical value $\Gamma < \Gamma_c$, states in the middle of the band are extended, while for $\Gamma \geqslant \Gamma_c$ all states in the band are localized. It has been shown [61–64] that localized states can also exist in the tails of the DOS of disordered materials. Based on these arguments, Mott [65] conjectured the existence of a threshold energy ("mobility edge"), at which a sharp transition from localized to extended states occurs.

In Fig. 1, we show the results for the average DOS $\rho(E) = c_{\rm Li}\rho^X_{\rm Li} + c_{\rm Be}\rho^X_{\rm Be}$ which is computed from the alloy components $\rho_{\rm Li}$ and $\rho_{\rm Be}$, where $X =$ CPA or TMT. Figure 1(a) corresponds to the DOS obtained for $X =$ CPA, where the alloy components are obtained from the CPA effective medium. The concentration varies in the range from 1% to 50%, and the bandwidth corresponds to a fixed value of the Wigner-Seitz radius $r_{\rm WS} = 3.50$ a.u. In the binary substitutional alloy Li_cBe_{1-c} the Li component has a reduced weight in comparison to the Be component for concentrations $c \leqslant 0.5$. In Fig. 1(b), we compare the DOS obtained for $X =$ CPA and $X =$ TMT.

The general structure of the DOS shown in Fig. 1 consists of two main DOS centered at $\epsilon_{\rm Li}$ and $\epsilon_{\rm Be}$, respectively. For the concentration range under consideration Be states form the "majority" (main) subband. As the concentration c is reduced, the impurity subband is split off from the main subband [Fig. 1(a)]. The same effect is also seen when the average DOS is computed from the alloys components provided by the TMT effective medium [Fig. 1(b)].

In our self-consistent framework, the total number of electrons is computed from the average DOS $\rho(E)$ of the alloy components. Therefore, the Fermi level calculated within the CPA is different from the value obtained when the typical medium is used. Within the CPA, Fig. 1(a), the Fermi level is pinned by the maximum of the impurity band, while using the typical medium, Fig. 1(b), the Fermi level lies between the main and the split-off band, and a pseudogap develops around E_F. We note that due to the charge redistribution, no split band can be seen in the average DOS calculated with the TMT. Instead, the shift accounts for the conservation of the total number of electrons. For all concentrations studied here, the width of the subbands are found to be reduced compared to the CPA results, which already indicates the appearance of localized states at the band-edges.

An important quantity monitoring the effects of Anderson localization [33–35] is the DOS obtained by the TMT (TMT-DOS) [33–35]. It corresponds to an order parameter of the metal-to-insulator transition and is calculated according to

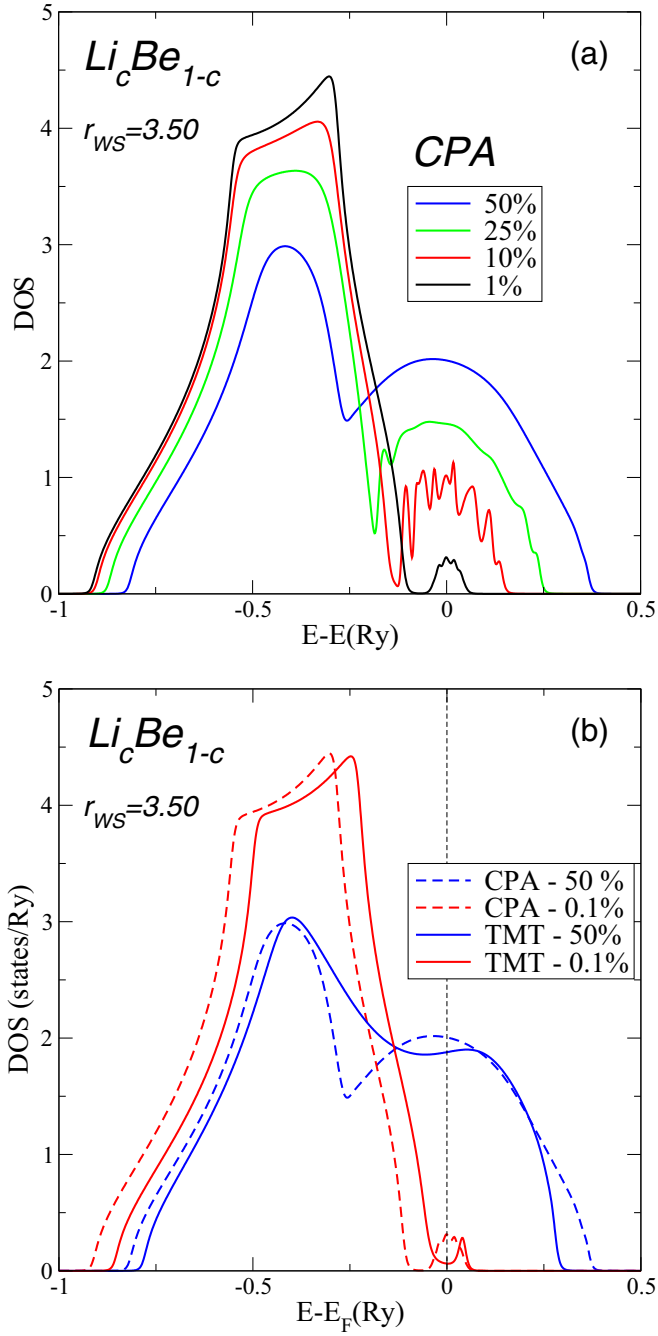

FIG. 1. (a) Average DOS of Li_cBe_{1-c} alloys calculated within CPA for different concentrations c for a given atomic Wigner-Seitz radius $r_{WS} = 3.50$ a.u., corresponding to a lattice parameter of 5.64 a.u. (= 2.98 Å). (b) Average DOS computed from the typical medium alloy components used in the charge self-consistent calculations.

Eq. (9) as

$$\rho(E) = [\rho_{\mathrm{Li}}(E)]^{c_{\mathrm{Li}}} \cdot [\rho_{\mathrm{Be}}(E)]^{c_{\mathrm{Be}}}. \tag{12}$$

Results are shown in Fig. 2. By decreasing the concentration of Li, the bandwidth is reduced due to Anderson localization. However, even for 1% of Li, the TMT-DOS at E_F does not reach zero. In the inset of Fig. 2, we present the comparison of the logarithms of CPA-DOS with that

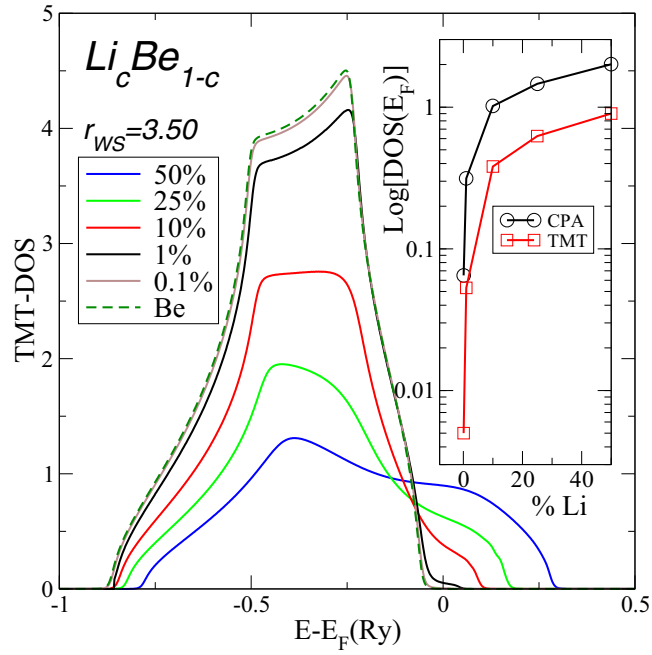

FIG. 2. The typical medium DOS (order parameter) of the Li_cBe_{1-c} alloy for different concentrations c of Li at the same value of $r_{WS} = 3.50$ a.u. (same bandwidth).

of the TMT-DOS. We see that at a concentration of 0.1%, the TMT-DOS is reduced by an order of magnitude. In this low concentration range, the shape of the TMT-DOS closely resembles that of bulk Be below 0.01%, see Fig. 2. Reducing the concentration further decreases the value of the TMT-DOS at E_F even more (see inset of Fig. 2).

In Fig. 3, we show the dependence of the TMT-DOS on the Wigner-Seitz radius (r_{WS}). Increasing r_{WS} corresponds to a larger lattice parameter. Expanding the unit cell leads to narrower bands. For r_{WS} in the range of 2.5 to 3.0 a.u. [Fig. 3(a)] the TMT-DOS is nonzero at the Fermi level, while a significant reduction is obtained for even larger values of r_{WS} [Fig. 3(b)].

B. Magnetism in doped MgO

The question whether, and how, impurity doping can stabilize band ferromagnetism has been extensively studied in the search for novel diluted magnetic semiconductors [66,67]. On general grounds, a substitution by an atom with reduced valency leads to hole doping which can shift the Fermi level into the valence band of the insulator or semiconductor. If the shift is sufficiently strong such that the Stoner criterion is fulfilled, spontaneous spin polarization sets in. Alternatively, substitution may introduce spin-polarized impurity states in the gap. When the concentration is increased the impurity states form bands, which remain spin-polarized. In the following, we illustrate this second scenario in the case of carbon substitution at the oxygen sites (Sec. IV B 1) and manganese substitution at the magnesium sites (Sec. IV B 2) in MgO. For the sake of completeness, we mention that there are other mechanisms beside spin polarization that may lift the degeneracy at the Fermi level, such as polaron formation

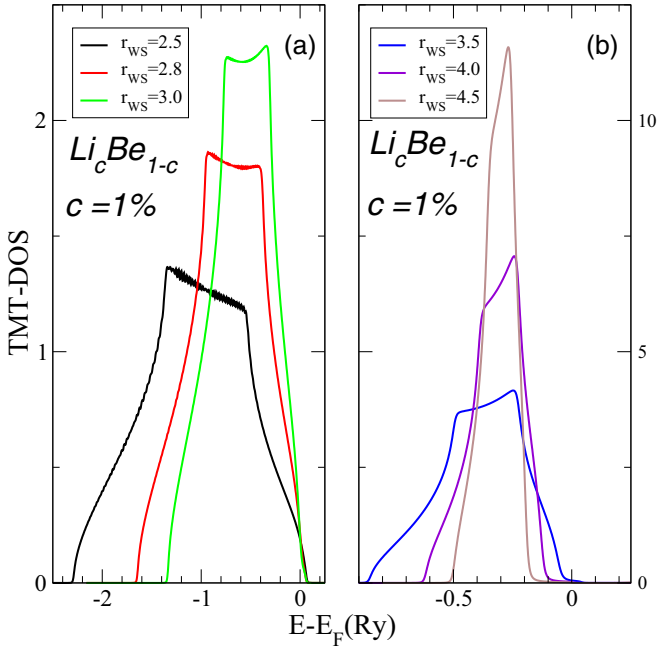

FIG. 3. The typical medium DOS (order parameter) of the Li_cBe_{1-c} alloys for different lattice parameters r_{WS} (different bandwidths) at the Li concentration $c = 1\%$. Note the factor five between the scales corresponding to the smaller (a) and larger (b) r_{WS}.

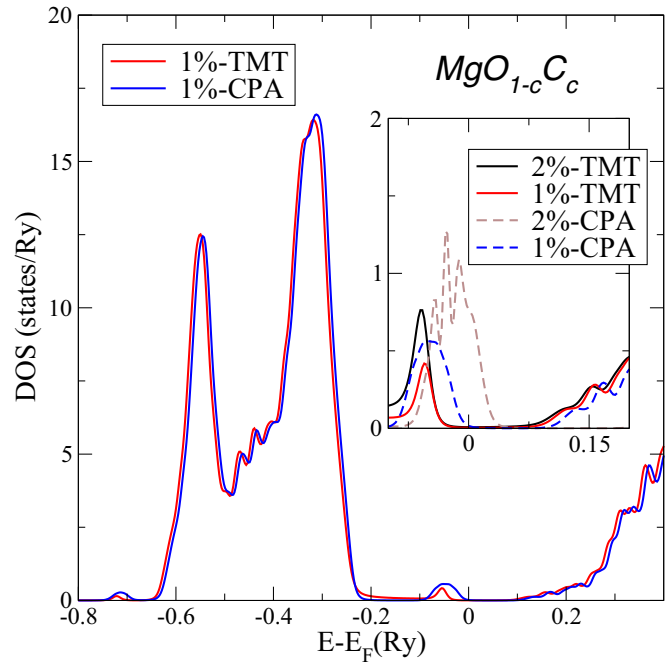

FIG. 4. Total DOS of $MgO_{1-c}C_c$ for $c = 1\%, 2\%$C. In the inset the TMT-DOS is compared with the DOS obtained using the effective medium of the CPA.

[68]. However, in the present paper we do not address this mechanism.

MgO is commonly employed as a substrate for thin-film growth of materials such as metals [69], nitrides [70], graphene [71], and high-T_c superconductors [72]. It also finds use as a barrier in magnetic tunnel junctions [73,74]. This makes MgO an important material for nanotechnologies and spintronic applications. Deviations from perfect crystallinity in MgO can have detrimental effects on its functionality. It was shown that poor-quality MgO substrates gives rise to poor-quality thin films [70], while defects and impurities can lead to a degradation of the superconducting properties in high-T_c superconductors [72,75]. On the other hand it is known that doping Fe/MgO/Fe tunnel junctions with carbon impurities increases the output voltage and reduces noise [76,77].

Under ambient conditions MgO crystallizes in the rock-salt (B1) structure with a measured lattice parameter $a_{\text{exp}} = 4.216$ Å, and has a large direct electronic band gap of about 7.8 eV [78–80]. In the following calculation, the experimental lattice parameter is used. The O-2s and O-2p states as well as the Mg-3s states are treated as valence states. In a simple picture the two valence s-electrons of Mg fill the O-2p shell. The bottom of the conduction band has almost pure Mg-3s character at the Γ-point, where the p-bands reach their maximum, making MgO a direct-gap insulator. While the local density approximation (LDA) is known to underestimate the gap of insulators and semiconductors [81], we obtain a direct band gap of 4.50 eV which is consistent with values from other investigations using similar approximations [82].

The EMTO method was successfully used to study the elastic and magnetic properties of pure and Fe-doped MgO [83]. We now explore other doping effects.

1. Carbon-doped MgO($MgO_{1-c}C_c$)

The electronic and magnetic properties of vacancies and nonmagnetic impurities in MgO have been investigated in detail for large impurity concentrations [84,85]. In particular, the polarization of the valence states of MgO by the substitution of oxygen with p-type impurities such as C and N [59,84] has been widely discussed. The typical experiments involve a high concentration of impurities. Consequently, the ferromagnetic interaction is mediated by partially occupied spin-polarized impurity states. In other words, the impurity states should be extended to mediate ferromagnetism, and at the same time the band width should be small enough such that the Stoner criterion is satisfied [60,86]. We note that in LDA and the generalized gradient approximation (GGA), the impurity 2p-states are too extended and the magnetism is overestimated for high concentrations [87,88]. Attempts to improve these results by including a Hubbard U within a Hartree mean-field decoupling (LDA + U or GGA + U approximations) or, alternatively, by including self-interaction corrections produce a splitting of the 2p-impurity levels and thereby lead to ferromagnetism. However, the local distortions around the defects due to the relaxation of the crystal structure inhibit magnetism [88,89]. A different mechanism for the formation of a magnetically ordered state, valid in the high concentration regime, is the formation of impurity pairs [84].

We now explore the opposite limit of very low concentrations ($0.01\% \leqslant c \leqslant 2\%$) when impurity states are well isolated. Then the question arises whether ferromagnetism is also found when localization effects are taken into account through the TMT approach. In Fig. 4, we show the DOS of MgO with 1% C impurities calculated for the CPA and TMT effective medium, respectively. Using the CPA effective

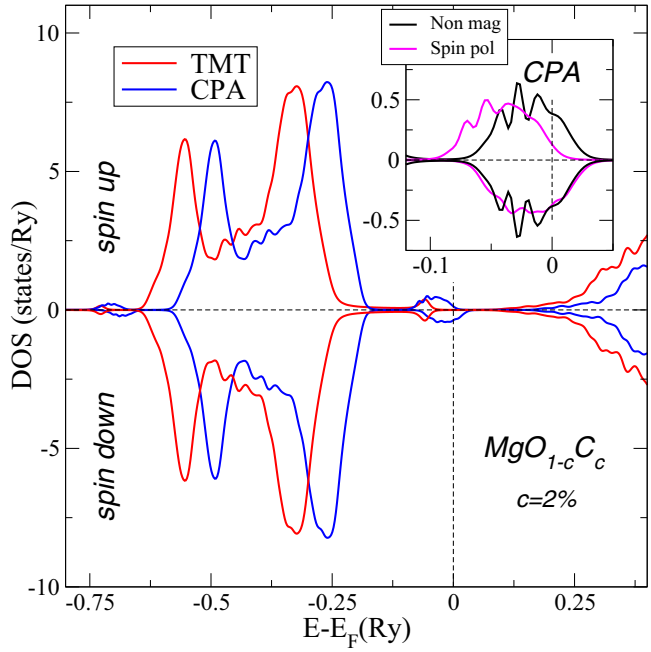

FIG. 5. Total DOS obtained with the spin-polarized CPA for 2% C substitution in $MgO_{0.98}C_{0.02}$ (blue line) and the nonmagnetic TMT solution (red line). Inset: Comparison of magnetic and nonmagnetic CPA solutions.

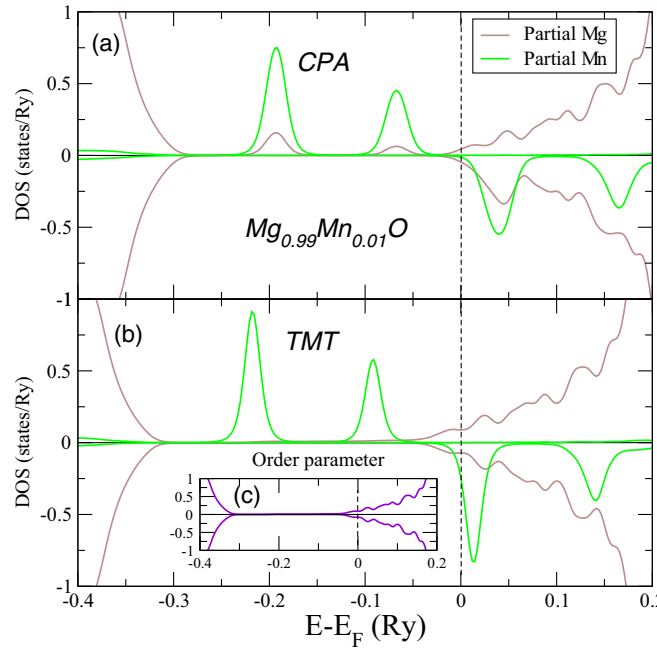

FIG. 6. (a) Spin-resolved CPA-DOS in the high-spin state for Mn-doped MgO. Brown/green curves correspond to Mg/Mn partial DOS, respectively. (b) TMT spin resolved partial DOS. Inset (c): Geometric average of the partial DOS (order parameter).

medium a nonvanishing value of the DOS at E_F is obtained. By contrast, a significantly reduced value of the DOS at the Fermi level is found in the TMT. In the inset of Fig. 4, the order parameter (TMT-DOS) is compared with the CPA-DOS for $c = 1\%$ and 2% C. At both concentrations the TMT-DOS is already zero, indicating an insulating state. At higher carbon concentrations, MgO has a magnetic ground state [84]. We notice that already for 2% carbon doping the ferromagnetic phase is lower in the total energy than the nonmagnetic one.

In Fig. 5, we show the DOS for $MgO_{0.98}C_{0.02}$ in the ferromagnetic phase computed within CPA together with the nonmagnetic solution obtained by the TMT. The inset of Fig. 5 shows a comparison of the CPA results in the nonmagnetic and ferromagnetic phase, respectively. In the ferromagnetic state, LDA predicts that the carbon acquires a nonzero magnetic moment of about 0.55 μ_B, which increases in GGA to about 0.95 μ_B. At 2.5% C the GGA produces an almost totally spin-polarized state with spin-up DOS merging the main band. By contrast, for the typical medium a stable magnetic solution was neither found in LDA or GGA.

2. *Manganese-doped* $\mathbf{MgO(Mg_{1-c}Mn_cO)}$

A half-metallic state was predicted for Mn-doped MgO, with Mn replacing Mg [90]. Both a high-spin ($S = 5/2$) and a low-spin ($S = 1/2$) state can be stabilized, with the high-spin state being insulating and the low-spin state being half-metallic [91]. The high-spin state is relevant for quantum information science since the system has been used to host qubits [92].

Doping with d electrons raises the question regarding the influence of $p - d$ hybridization upon the magnetism in the $Mg_{1-c}Mn_cO$ alloy. On general grounds, the p and d bands are coupled by the hybridization and disorder effects through the effective medium potential. Quite generally, the hybridization determines the relative band shifts, while disorder broadens the shifted bands. Magnetism depends on the d occupations. Due to the disorder, the fluctuation of the number of particles will influence the propagation of electrons and thus change the DOS. Since the fluctuation is spin dependent, it affects the spin-up and -down DOS differently and thereby directly influences the spin asymmetry.

In Fig. 6(a), the spin-resolved DOS for MgO doped with 1% Mn as computed with CPA (upper panel) and TMT (lower panel), is shown. The Mn d-states are located in the gap of MgO and are split according to the cubic crystal field: the triply degenerate t_{2g} states are located at about -0.2 Ry and the doubly degenerate e_g states at about -0.1 Ry. In this case, the ground state corresponds to the high-spin solution with both spin-up t_{2g} and e_g states being completely filled, while the spin-down t_{2g} and e_g states are shifted above the Fermi level. Note that the partial Mg and Mn DOS obtained within the CPA shows overlapping maxima at the same energies as a consequence of significant $p - d$ hybridization. The position of the maxima corresponds to the shifted one-particle energies because of hybridization. The value of the Mn magnetic moment is 3.8 μ_B and corresponds to the $S = 5/2$ state. By contrast, the DOS obtained within the TMT, Fig. 6(b), shows no overlap of p and d orbitals, and the total DOS within the gap is determined only by Mn d-orbitals. The absence of hybridization leads to a shift of the t_{2g} and e_g states. The Mn total magnetic moment is 3.8 μ_B. The inset of Fig. 6(b) shows the geometric average of the LDOS (at the Mg site), which represents the order parameter. On the level of the DOS, the

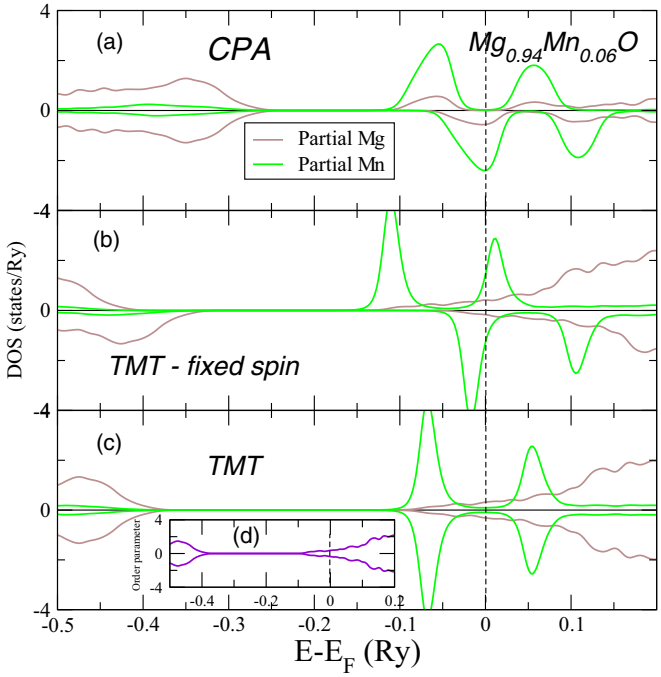

FIG. 7. (a) Spin-resolved CPA-DOS in the low-spin state. Brown/green curves correspond to Mg/Mn partial DOS, respectively. Fixed-spin (b) and unbiased spin polarized calculation (c) using the TMT. Inset (d): Geometric average of partial DOS (order parameter).

self-consistent TMT effective medium calculation leads to a cancellation of the $p-d$ hybridization.

Figure 7(a) shows the CPA solution for the low-spin state in the case of 6% Mn doping. Here the majority t_{2g} states are completely filled and the minority t_{2g} states are partially occupied. The e_g states are empty in both spin channels. The resulting state is half-metallic with a spin $S = 1/2$. No low-spin magnetic configuration is found within the TMT. Instead, by fixing the total spin to the expected low-spin solution ($0.06\,\mu_B$), the TMT converges to a state with a DOS shown in Fig. 7(b). Since the fixed-spin solution was allowed to relax, the system converges to a non-magnetic solution [see Fig. 7(c)]. In both TMT computations, Figs. 7(b) and 7(c), no overlap between the p and d orbitals is found.

We now summarize the comparison between the CPA and TMT results in the case of $Mg_{1-c}Mn_cO$. The question if, and how, the p-d hybridization contributes to the magnetic properties of this alloy can indeed be answered. In the case of CPA the p-d hybridization is present and both the low- and high-spin magnetic configurations are possible. However, within the TMT, the high-spin state remains magnetic with no significant difference compared with the corresponding CPA solution, despite the suppressed p-d hybridization. Furthermore, no low-spin magnetic configuration is obtained using the TMT effective medium. The destabilization of the low-spin solution results from the spin-dependent particle fluctuations between p and d states, due to disorder. In fact, both CPA and TMT have such effects included through the effective medium "self-energy" which renormalizes the quasiparticle DOS. This renormalization can be analyzed in terms of band broadening and band shifts. The interband fluctuations are found to have considerable influence on the magnetic properties of the low-spin configuration. Namely, these weak magnetic effects remain for weak disorder (CPA), but are suppressed by strong disorder (TMT).

V. CONCLUSION

We implemented the effective TMT within the DFT by employing the EMTO-basis set and compared the results obtained thereby with those of the CPA. The framework was then applied to study the evolution of the impurity band appearing in the hypothetical Li_cBe_{1-c} alloy, a simple cubic system with one-atom per unit cell. This alloy system was studied within DFT and different effective medium theories. The DOS results show signatures of Anderson localization effects, band narrowing and split-off impurity bands. We also discussed the effect of charge self-consistency and the determination of the Fermi level E_F. The search for E_F is implemented in a similar way as in the CPA case, with the difference that the average DOS is constructed from the alloy components computed with the typical medium path operators. Furthermore, we studied the magnetic properties of dilute $MgO_{1-c}C_c$ and $Mg_{1-c}Mn_cO$ alloys. In contrast to the carbon substitution in MgO, the Mn substitution brings into the discussion the presence of d orbitals and their contribution to the magnetism of Mn impurities. We found that disorder-induced interband particle number fluctuations suppress magnetism together with the p-d hybridization in the case of low-spin configurations. In the charge self-consistent calculations, the system lowers its energy by particle fluctuations. Since these fluctuations are spin dependent, they influence the magnetic stability of the system.

The implementation of the effective TMT within the DFT presented in this paper can be generalized to include electronic correlation effects through the dynamical mean-field theory (DMFT). This opens the possibility for *ab initio* studies of correlated electron materials in the presence of disorder beyond CPA.

ACKNOWLEDGMENTS

This work was supported by the U.S. Department of Energy, Office of Science, Office of Basic Energy Sciences under Award No. DE-SC0017861. Financial support offered by the Augsburg Center for Innovative Technologies, and by the Deutsche Forschungsgemeinschaft (DFG), Project No. 107745057–TRR 80/F6, is gratefully acknowledged. H.T. gratefully acknowledges support from NSF Grant No. CSSI-1931367. L.V. acknowledges financial support from the Swedish Research Council, the Swedish Foundation for Strategic Research, the Swedish Foundation for International Cooperation in Research and Higher Education, and the Hungarian Scientific Research Fund (OTKA 84078). We acknowledge computational resources provided by the Swedish National Infrastructure for Computing (SNIC) at the National Supercomputer Centre (NSC) in Linköping.

[1] J. M. Ziman, *Models of Disorder* (Cambridge University Press, Cambridge, 1979).
[2] P. A. Lee and T. V. Ramakrishnan, Rev. Mod. Phys. **57**, 287 (1985).
[3] D. Belitz and T. R. Kirkpatrick, Rev. Mod. Phys. **66**, 261 (1994).
[4] P. Hohenberg and W. Kohn, Phys. Rev. **136**, B864 (1964).
[5] W. Kohn and L. J. Sham, Phys. Rev. **140**, A1133 (1965).
[6] W. Kohn, Rev. Mod. Phys. **71**, 1253 (1999).
[7] R. O. Jones and O. Gunnarsson, Rev. Mod. Phys. **61**, 689 (1989).
[8] R. O. Jones, Rev. Mod. Phys. **87**, 897 (2015).
[9] R. J. Elliott, J. A. Krumhansl, and P. L. Leath, Rev. Mod. Phys. **46**, 465 (1974).
[10] P. Soven, Phys. Rev. **156**, 809 (1967).
[11] D. W. Taylor, Phys. Rev. **156**, 1017 (1967).
[12] B. Velický, S. Kirkpatrick, and H. Ehrenreich, Phys. Rev. **175**, 747 (1968).
[13] B. L. Gyorffy, Phys. Rev. B **5**, 2382 (1972).
[14] L. Vitos, P. A. Korzhavyi, and B. Johansson, Phys. Rev. Lett. **88**, 155501 (2002).
[15] J. S. Faulkner and G. M. Stocks, Phys. Rev. B **21**, 3222 (1980).
[16] J. S. Faulkner and T. P. Beaulac, Phys. Rev. B **26**, 1597 (1982).
[17] D. D. Johnson, D. M. Nicholson, F. J. Pinski, B. L. Gyorffy, and G. M. Stocks, Phys. Rev. Lett. **56**, 2088 (1986).
[18] P. Weinberger, V. Drchal, L. Szunyogh, J. Fritscher, and B. I. Bennett, Phys. Rev. B **49**, 13366 (1994).
[19] P. P. Singh, A. Gonis, and P. E. A. Turchi, Phys. Rev. Lett. **71**, 1605 (1993).
[20] D. D. Johnson, D. M. Nicholson, F. J. Pinski, B. L. Györffy, and G. M. Stocks, Phys. Rev. B **41**, 9701 (1990).
[21] B. Magyari-Köpe, G. Grimvall, and L. Vitos, Phys. Rev. B **66**, 064210 (2002).
[22] B. Magyari-Köpe, G. Grimvall, and L. Vitos, Phys. Rev. B **66**, 179902(E) (2002).
[23] A. Östlin, L. Vitos, and L. Chioncel, Phys. Rev. B **98**, 235135 (2018).
[24] A. Gonis and J. W. Garland, Phys. Rev. B **18**, 3999 (1978).
[25] A. Gonis, *Green Functions for Ordered and Disordered Systems* (North-Holland, Amsterdam, 1992).
[26] M. Jarrell and H. R. Krishnamurthy, Phys. Rev. B **63**, 125102 (2001).
[27] D. A. Rowlands, J. B. Staunton, and B. L. Györffy, Phys. Rev. B **67**, 115109 (2003).
[28] D. A. Biava, S. Ghosh, D. D. Johnson, W. A. Shelton, and A. V. Smirnov, Phys. Rev. B **72**, 113105 (2005).
[29] D. A. Rowlands, J. B. Staunton, B. L. Györffy, E. Bruno, and B. Ginatempo, Phys. Rev. B **72**, 045101 (2005).
[30] D. A. Rowlands, A. Ernst, B. L. Györffy, and J. B. Staunton, Phys. Rev. B **73**, 165122 (2006).
[31] P. W. Anderson, Phys. Rev. **109**, 1492 (1958).
[32] For discussions, see Refs. [34,93,94].
[33] G. Schubert, J. Schleede, K. Byczuk, H. Fehske, and D. Vollhardt, Phys. Rev. B **81**, 155106 (2010).
[34] V. Dobrosavljević, A. A. Pastor, and B. K. Nikolić, Europhys. Lett. **62**, 76 (2003).
[35] V. Dobrosavljević, Int. J. Mod. Phys. B **24**, 1680 (2010).
[36] S. Mahmoudian, S. Tang, and V. Dobrosavljević, Phys. Rev. B **92**, 144202 (2015).
[37] M. C. O. Aguiar, V. Dobrosavljević, E. Abrahams, and G. Kotliar, Phys. Rev. Lett. **102**, 156402 (2009).
[38] M. C. O. Aguiar and V. Dobrosavljević, Phys. Rev. Lett. **110**, 066401 (2013).
[39] H. Braganca, M. C. O. Aguiar, J. Vučičević, D. Tanasković, and V. Dobrosavljević, Phys. Rev. B **92**, 125143 (2015).
[40] M. C. O. Aguiar, V. Dobrosavljević, E. Abrahams, and G. Kotliar, Phys. Rev. B **73**, 115117 (2006).
[41] C. E. Ekuma, H. Terletska, K.-M. Tam, Z.-Y. Meng, J. Moreno, and M. Jarrell, Phys. Rev. B **89**, 081107(R) (2014).
[42] H. Terletska, Y. Zhang, K.-M. Tam, L. Berlijn, T. Chioncel, N. S. Vidhyadhiraja, and M. Jarrell, Appl. Sci. **8**, 2401 (2018).
[43] H. Terletska, C. E. Ekuma, C. Moore, K.-M. Tam, J. Moreno, and M. Jarrell, Phys. Rev. B **90**, 094208 (2014).
[44] Y. Zhang, H. Terletska, C. Moore, C. Ekuma, K.-M. Tam, T. Berlijn, W. Ku, J. Moreno, and M. Jarrell, Phys. Rev. B **92**, 205111 (2015).
[45] C. E. Ekuma, S.-X. Yang, H. Terletska, K.-M. Tam, N. S. Vidhyadhiraja, J. Moreno, and M. Jarrell, Phys. Rev. B **92**, 201114(R) (2015).
[46] H. Terletska, Y. Zhang, L. Chioncel, D. Vollhardt, and M. Jarrell, Phys. Rev. B **95**, 134204 (2017).
[47] Y. Zhang, R. Nelson, E. Siddiqui, K.-M. Tam, U. Yu, T. Berlijn, W. Ku, N. S. Vidhyadhiraja, J. Moreno, and M. Jarrell, Phys. Rev. B **94**, 224208 (2016).
[48] Y. Zhang, R. Nelson, K.-M. Tam, W. Ku, U. Yu, N. S. Vidhyadhiraja, H. Terletska, J. Moreno, M. Jarrell, and T. Berlijn, Phys. Rev. B **98**, 174204 (2018).
[49] For the definition of the PDF function within the muffin-tin formalism, see Refs. [55,56].
[50] J. Korringa, Physica **13**, 392 (1947).
[51] W. Kohn and N. Rostoker, Phys. Rev. **94**, 1111 (1954).
[52] P. Weinberger, *Electron Scattering Theory for Ordered and Disordered Matter* (Clarendon Press, Oxford, 1990).
[53] F. S. Ham and B. Segall, Phys. Rev. **124**, 1786 (1961).
[54] J. S. Faulkner, H. L. Davis, and H. W. Joy, Phys. Rev. **161**, 656 (1967).
[55] O. K. Andersen, Phys. Rev. B **12**, 3060 (1975).
[56] H. L. Skriver, *The LMTO Method* (Springer-Verlag, Berlin, 1984).
[57] O. K. Andersen and T. Saha-Dasgupta, Phys. Rev. B **62**, R16219(R) (2000).
[58] L. Vitos, Phys. Rev. B **64**, 014107 (2001).
[59] I. S. Elfimov, A. Rusydi, S. I. Csiszar, Z. Hu, H. H. Hsieh, H.-J. Lin, C. T. Chen, R. Liang, and G. A. Sawatzky, Phys. Rev. Lett. **98**, 137202 (2007).
[60] V. Pardo and W. E. Pickett, Phys. Rev. B **78**, 134427 (2008).
[61] I. Lifshitz, Adv. Phys. **13**, 483 (1964).
[62] B. I. Halperin and M. Lax, Phys. Rev. **148**, 722 (1966).
[63] J. Zittartz and J. S. Langer, Phys. Rev. **148**, 741 (1966).
[64] A. B. Harris and R. V. Lange, Phys. Rev. **157**, 295 (1967).
[65] N. Mott, Adv. Phys. **16**, 49 (1967).
[66] K. Sato, L. Bergqvist, J. Kudrnovský, P. H. Dederichs, O. Eriksson, I. Turek, B. Sanyal, G. Bouzerar, H. Katayama-Yoshida, V. A. Dinh, T. Fukushima, H. Kizaki, and R. Zeller, Rev. Mod. Phys. **82**, 1633 (2010).
[67] T. Dietl and H. Ohno, Rev. Mod. Phys. **86**, 187 (2014).
[68] S. Kokott, S. V. Levchenko, P. Rinke, and M. Scheffler, New J. Phys. **20**, 033023 (2018).
[69] R. Hoel, Surf. Sci. **169**, 317 (1986).
[70] J. L. Schroeder, A. S. Ingason, J. Rosén, and J. Birch, J. Cryst. Growth **420**, 22 (2015).

[71] L. Kong, C. Bjelkevig, S. Gaddam, M. Zhou, Y. H. Lee, G. H. Han, H. K. Jeong, N. Wu, Z. Zhang, J. Xiao, P. A. Dowben, and J. A. Kelber, J. Phys. Chem. C **114**, 21618 (2010).
[72] B. H. Moeckly, S. E. Russek, D. K. Lathrop, R. A. Buhrman, J. Li, and J. W. Mayer, Appl. Phys. Lett. **57**, 1687 (1990).
[73] S. S. P. Parkin, C. Kaiser, A. Panchula, P. M. Rice, B. Hughes, M. Samant, and S.-H. Yang, Nat. Mater. **3**, 862 (2004).
[74] S. Ikeda, J. Hayakawa, Y. Ashizawa, Y. M. Lee, K. Miura, H. Hasegawa, M. Tsunoda, F. Matsukura, and H. Ohno, Appl. Phys. Lett. **93**, 082508 (2008).
[75] S. Karimoto, H. Sato, and T. Makimoto, Jpn. J. Appl. Phys. **45**, L419 (2006).
[76] C. Tiusan, M. Sicot, M. Hehn, C. Belouard, S. Andrieu, F. Montaigne, and A. Schuhl, Appl. Phys. Lett. **88**, 062512 (2006).
[77] D. Herranz, R. Guerrero, J. Cascales, F. Aliev, and M. Hehn, Acta Phys. Pol. A **121**, 981 (2012).
[78] D. M. Roessler and W. C. Walker, Phys. Rev. **159**, 733 (1967).
[79] M. W. Williams and E. T. Arakawa, J. Appl. Phys. **38**, 5272 (1967).
[80] S. Kowalczyk, F. McFeely, L. Ley, V. Gritsyna, and D. Shirley, Solid State Commun. **23**, 161 (1977).
[81] J. P. Perdew and M. Levy, Phys. Rev. Lett. **51**, 1884 (1983).
[82] B. B. Karki, L. Stixrude, S. J. Clark, M. C. Warren, G. J. Ackland, and J. Crain, Am. Miner. **82**, 51 (1997).
[83] L. Koči, L. Vitos, and R. Ahuja, Phys. Earth Planet. Inter. **164**, 177 (2007).
[84] H. Wu, A. Stroppa, S. Sakong, S. Picozzi, M. Scheffler, and P. Kratzer, Phys. Rev. Lett. **105**, 267203 (2010).
[85] I. Slipukhina, P. Mavropoulos, S. Blügel, and M. Ležaić, Phys. Rev. Lett. **107**, 137203 (2011).
[86] H. Peng, H. J. Xiang, S.-H. Wei, S.-S. Li, J.-B. Xia, and J. Li, Phys. Rev. Lett. **102**, 017201 (2009).
[87] D. A. Papaconstantopoulos, W. E. Pickett, B. M. Klein, and L. L. Boyer, Phys. Rev. B **31**, 752 (1985).
[88] J. A. Chan, S. Lany, and A. Zunger, Phys. Rev. Lett. **103**, 016404 (2009).
[89] A. Droghetti, C. D. Pemmaraju, and S. Sanvito, Phys. Rev. B **78**, 140404(R) (2008).
[90] V. Sharma, G. Pilania, and J. E. Lowther, AIP Adv. **1**, 032129 (2011).
[91] S. Meskine, A. Boukortt, R. Hayn, and A. Zaoui, Phys. Status Solidi B **251**, 845 (2014).
[92] S. Bertaina, L. Chen, N. Groll, J. Van Tol, N. S. Dalal, and I. Chiorescu, Phys. Rev. Lett. **102**, 050501 (2009).
[93] K. Byczuk, W. Hofstetter, and D. Vollhardt, Phys. Rev. Lett. **94**, 056404 (2005).
[94] K. Byczuk, W. Hofstetter, and D. Vollhardt, in *Fifty Years of Anderson Localization*, edited by E. Abrahams (World Scientific, Singapore, 2010), p. 473 [reprinted in Int. J. Mod. Phys. B **24**, 1727 (2010)].